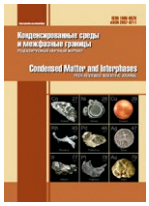

ISSN 1606-867X (Print)
ISSN 2687-0711 (Online)
Condensed Matter and Interphases
Kondensirovannye Sredy i Mezhfaznye Granitsy
https://journals.vsu.ru/kcmf/

Original articles

Research article
https://doi.org/10.17308/kcmf.2023.25/11110

Phase relations in the Si–Sn–As system

T. P. Sushkova✉, G. V. Semenova, E. Yu. Proskurina

[1]Voronezh State University,
1 Universitetskaya pl., Voronezh 394018, Russian Federation

[2]Voronezh State Technical University,
84 20 letiya Oktyabrya st., Voronezh, 394006, Russian Federation

Abstract

The goal of this work was to study phase relations in the ternary Si–Sn–As system: to establish cross sections, to construct a scheme of phase equilibria, and to identify the temperature of non-variant transformations.

Ternary alloys were obtained through direct synthesis from simple substances and subjected to long-term solid-phase annealing. Alloys of four polythermal sections of the Si–Sn–As system were examined using X-ray phase and differential thermal analysis. The results of X-ray powder diffraction allowed establishing that the phase subsolidus demarcations was performed by the $SnAs–SiAs_2$, SnAs–SiAs, Sn_4As_3–SiAs, and Sn_4As_3–Si sections.

As a result of the experiment, taking into account the theoretical analysis, we suggested a scheme of phase equilibria in the system that involved the implementation of eutectic and four peritectic invariant equilibria, and we used differential thermal analysis to determine the temperature of these four-phase transformations.

It was found that extended solid solutions were not formed in the system, and only a substitutional solid solution at least 3 mol % wide was formed based along the $SnAs–SiAs_2$ section based on tin monoarsenide.

Keywords: Phase diagram, Polythermal section, Si–Sn–As ternary system

Acknowledgements: X-ray powder diffraction studies were performed using the equipment of the VSU Centre for Collective Use of Scientific Equipment.

For citation: Sushkova T. P., Semenova G. V., Proskurina E. Yu. Phase relations in the Si–Sn–As system. *Condensed Matter and Interphases*. 2023;25(2): 237–248. https://doi.org/10.17308/kcmf.2023.25/11110

Для цитирования: Сушкова Т. П., Семенова Г. В., Проскурина Е. Ю. Фазовые отношения в системе Si–Sn–As. Конденсированные среды и межфазные границы. 2023;25(2): 237–248. https://doi.org/10.17308/kcmf.2023.25/11110

✉ Tatiana P. Sushkova, e-mail: sushtp@yandex.ru

1. Introduction

Compounds of the $A^{IV}B^{V}$ class in the form of bulk single and polycrystals have been actively studied since the 1970s, and the Department of General and Inorganic Chemistry of Voronezh State University also performed such studies [1–4]. Although some of these compounds possess semiconductor properties and electrophysical characteristics that are practically important, they had not been put to good use for a long time. This is mainly associated with the fact that many $A^{IV}B^{V}$ compounds have a layered structure and can stratify into flakes when crystals are cut and ground, which was considered a significant drawback in the era of wide use of diamond-like semiconductors.

Over the past 20 years, due to the rapid development of 2D technologies, researchers have again turned their attention to this class of compounds. Silicon and germanium monopnictides form a family of two-dimensional layered semiconductors with a possibility of changing the width of the band gap through the variation of the number of layers [5–8]. They can also be used as catalysts and materials for optoelectronic devices [9–11]. The peeling energy of silicon and germanium arsenides and phosphides can be compared to this value for graphene, which suggests a high probability of their successful production using mechanical peeling from bulk crystals [5, 6].

Bulk crystals of $A^{IV}B^{V}$ compounds also have practical importance as they are capable of interlayer introduction reactions. Tin and silicon arsenides SnAs, Sn_4As_3, $SiAs_2$, and SiAs are suitable materials for the creation of electrodes of alkali-ion batteries [12–14]. For example, Li_2SiAs_2 has a calculated band gap of 1.4 eV, low thermal conductivity at room temperature, and high electrical resistivity, and therefore it is highly promising as a lithium-ion conductor with lithium-ion conductivity at room temperature of 7 μΩ/cm [13].

Functional properties of the material can be improved to some extent through doping and the use of solid solutions instead of pure compounds. From this point of view, it is important to study the phase diagrams of multicomponent systems formed by the elements of the IVA and VA groups. The phase diagrams of $A^{IV}–B^{V}–C^{V}$ systems with anionic substitution have been studied better as compared to the diagrams of the systems with cationic substitution [15, 16]. There are no publications on the state diagram of the Si–Sn–As system, which explains the relevance of this work

The goal of this work was theoretical analysis and experimental study of phase relations in a ternary Si–Sn–As system: establishing cross sections, constructing a scheme of phase equilibria, and identifying the temperature of non-variant transformations.

2. Experimental

2.1. Methods for Sample Synthesis

Due to the high melting point of silicon, which cannot be reached upon synthesis in quartz tubes, as well as the duration of the solid phase reaction and considerable vapour pressure of arsenic at high temperatures, the experimental study of the phase diagram of Si–Sn–As becomes a challenging process.

The samples with the compositions belonging to four polythermal sections of the $SnAs–SiAs_2$, SnAs–SiAs, SnAs–Si, and SiAs–Sn ternary system were obtained by synthesis in a single zone furnace from simple substances in quartz ampoules vacuumed to the residual pressure of $5·10^{-4}$ GPa. KEF 4.5/0.1-43.5 silicon, OVCH-000, and OSCH-9-5 arsenic were used for the synthesis. Arsenic was preliminary purified from oxides using vacuum sublimation. The weighing was performed on AR2140 electronic scales with the measurement error $±1·10^{-3}$ g.

Maximum temperature of the furnace heating upon synthesis was 1353 K, which is lower than the melting point of silicon (1683 K). To ensure the possibility of the heterogeneous reaction, the samples were held for six hours at 1353 K and after the synthesis they were subject to solid phase annealing for 250 hours at 753 K (the alloys of the SiAs–Sn section rich in tin were annealed at 473 K).

To make sure that the temperature and the duration of synthesis and annealing are enough for the silicon to react, a binary alloy was prepared in similar conditions, the composition of which $Si_{0.48}As_{0.52}$ corresponded to the eutectic mixture of $SiAs_2$ and SiAs in the Si–As binary system. Peaks of silicon monoarsenide and diarsenide were observed on an X-ray diffraction pattern of this alloy while there were now silicon peaks. Therefore, the temperature and duration of synthesis and

annealing are enough for silicon to react completely in the conditions of our experiment.

2.2. Methodology of X-ray diffraction and differential thermal analysis

The alloys were studied using X-ray diffraction analysis (XRD) and differential thermal analysis (DTA).

X-ray phase analysis was performed using an ARL X'TRA diffractometer with Bragg–Brentano Θ–Θ focusing geometry. The source of radiation was an X-ray tube with a copper anode: $\lambda(\text{Cu-}K_{\alpha 1})$ = 0.1541 nm; $\lambda(\text{Cu-}K_{\alpha 2})$ = 0.1544 nm. The X-ray patterns were made with a step size of 0.04° and a counting time of 3 seconds per step. The determination error for the interplanar distances d_{hkl} was below $5 \cdot 10^{-4}$ nm. Parameters of the lattice of the phases were calculated using High Score Plus-305 program and specified using the Pauli principle.

Differential thermal analysis was performed on a DTA device with the programmed furnace heating with a heating rate 5 K/min (7 K/min for the most refractory samples). Heat treated chromel-alumel thermocouples and aluminium oxide were used as a reference. The signal received from the thermocouples was digitized and processed by the MasterSCADA software package. The determination error for the temperature of phase transformations was below ±1 K. The alloys of the studied system had a tendency to overcool, therefore the temperature of phase transitions was determined by the heating curves. In cases where the peak corresponding to the liquidus on a thermogram was stretched and fuzzy, the temperature was determined by the cooling curve with a correction for the overcooling value.

3. Results and discussion

3.1. Results of an X-ray study and a scheme of phase equilibria in a ternary system

As we were studying the Si–Sn–As ternary system for the first time, it was necessary to analyse the possibility of its separation into subsystems using cross sections.

Two intermediate compounds were formed in the Si–As binary system: silicon monoarsenide that had a monoclinic crystal lattice and melted congruently at a temperature of 1386 K, and silicon diarsenide with an orthorhombic lattice, which decomposed according to the peritectic scheme into SiAs and a melt at 1250 K [17]. Silicon monoarsenide was a one-sided phase shifted towards silicon, while the stoichiometric composition practically coincided with the right border of the homogeneity region. The width of the homogeneity region of SiAs was 0.45 mol % at 1300 K [4,15]. Arsenic dissolves well in silicon, and the maximum solid phase solubility is about 3.5 mol % As at ~1473 K [17].

In the Sn–As system, two intermediate phases were also formed [18]: tin monoarsenide with a crystal lattice of the NaCl type and Sn_4As_3 which melted congruently at 868 K and crystallised in the trigonal non-centrosymmetrical space group $R\bar{3}m$, while the selected unit cell could be either rhombohedral or hexagonal [19]. Sn_4As_3 had a pronounced homogeneity region (~3 mol %) directed towards the excess of tin [18]. In the Si–Sn system [20] there were no intermediate compounds, and a degenerate eutectic near tin was observed with a temperature of 231.9 °C, which was similar to the melting point of pure tin. Tin slightly dissolved in silicon, and the maximum solid phase solubility was 0.1 mol % achieved at a temperature of 1339 K.

Therefore, due to the nature of the melting of intermediate phases and the presence of visible regions of homogeneity in some of them, only subsolidus phase separation was possible. Figure 1 shows four possible options for the division of a ternary system by cross sections (below the solidus) into subsystems, each of which had three solid phases coexisting in equilibrium.

Arsenic can participate in equilibria with the closest phases SnAs and $SiAs_2$, which means that a part of the concentration triangle with As the apex is separated in the only possible way. As an example, Figure 2a shows the X-ray powder diffraction spectrum of an alloy of the SnAs–$SiAs_2$ section alloy containing 20 mol % $SiAs_2$. Peaks of silicon diarsenide and tin monoarsenide were observed, and the intensity of the peaks of the second phase were higher as it prevailed in this alloy. It should be noted that the $(SnAs)_{0.97}(SiAs_2)_{0.03}$ sample was single-phase, while $((SnAs)_{0.93}(SiAs_2)_{0.07}$ was a two-phase sample, which probably indicated the formation of a solid solution based on SnAs with a range of at least 3 mol % along the SnAs–$SiAs_2$ section.

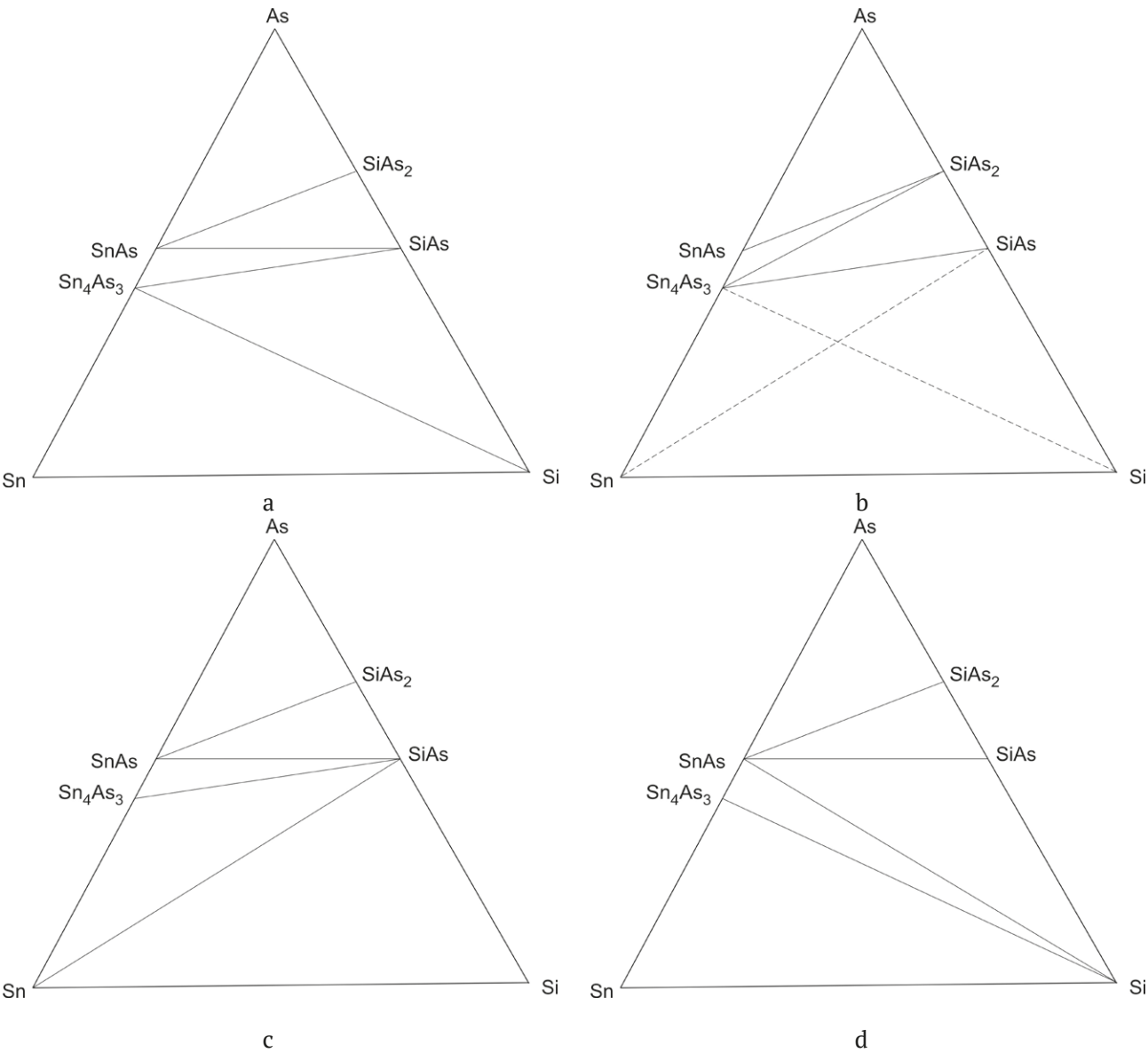

Fig. 1. Schemes of phase equilibria in the Si–Sn–As ternary system

Table 1 shows the cubic lattice parameter (a) and unit cell volume (*V*) of the SnAs phase which is present in the alloys of the polythermal section SnAs–$SiAs_2$. Parameters of the lattice were calculated using High Score Plus-305 program and specified using the Pauli principle. Both the lattice parameter and the cell volume were slightly decreased as compared to the data for tin monoarsenide presented in the powder X-ray diffraction catalogue (PDF2-2012 database). This indicated the formation of a solid substitution solution (tin atoms were replaced by smaller silicon atoms). The parameters of the orthorhombic $SiAs_2$ lattice differed very little from the reference values.

The Sn_4As_3–SnAs–$SiAs_2$–SiAs trapezium could be divided into triangles corresponding to the equilibrium of three solid phases using two methods: the SnAs–SiAs cross section (Fig. 1a) or the Sn_4As_3–$SiAs_2$ cross section (Fig. 1b). If the second scheme is correct, the alloys whose compositions belong to the SnAs–SiAs section and are to the right of the crossing point with the Sn_4As_3–$SiAs_2$ section should not contain tin monoarsenide and should contain Sn_4As_3. X-ray phase analysis showed that, on the contrary, SnAs was present in these alloys, while Sn_4As_3 was not, therefore, the scheme presented in Fig. 1b had to be excluded from consideration.

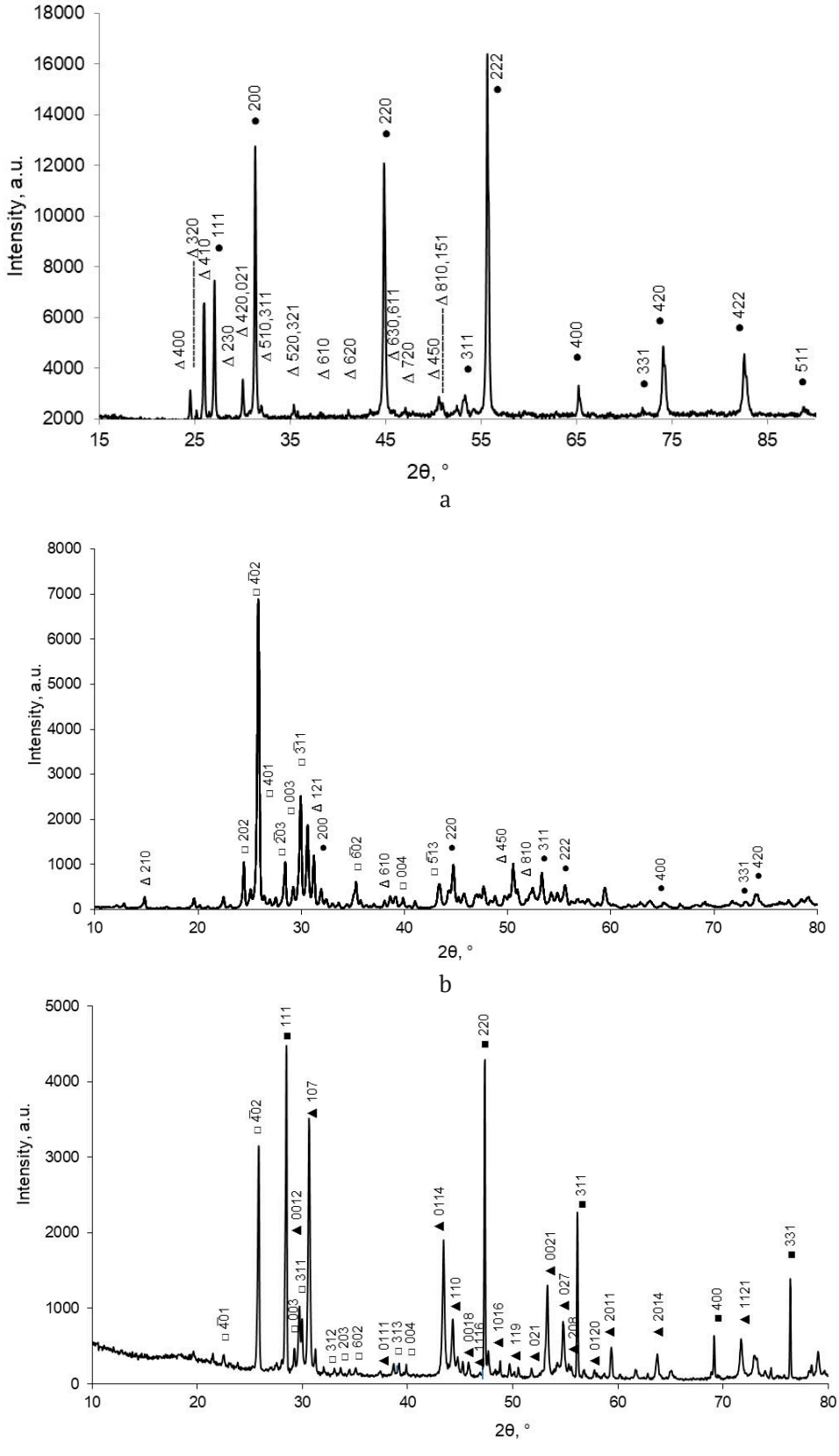

Fig. 2. X-ray powder diffraction patterns of the Si–Sn–As system: a – $(SnAs)_{0.8}(SiAs_2)_{0.2}$; b – $(SnAs)_{0.4}(SiAs)_{0.6}$; c – $(SnAs)_{0.8}Si_{0.2}$. Phase symbols: ■ – Si, ● – SnAs, □ – SiAs, Δ– $SiAs_2$, ▲ – Sn_4As_3

Table 1. Lattice parameter and unit cell volume of tin monoarsenide present in the alloys of the SnAs–$SiAs_2$ section

PDF2 data		Composition of the alloys, mol f., $SiAs_2$				
SnAs		0.03	0.07	0.2	0.4	0.6
a, Å	5.7248	5.7245	5.7206	5.7225	5.7217	5.7212
$V/10^6$ pm^3	187.621	187.591	187.208	187.391	187.315	187.268

The cubic phase of SnAs did not have many peaks but almost all of them were observed on diffraction patterns. Fig. 2b shows an X-ray diffraction spectrum of an alloy $(SnAs)_{0.4}(SiAs)_{0.6}$. Apart from the SnAs and SiAs peaks, several peaks of tin diarsenide could be observed. This is how we explain this fact: the process of crystallisation of the $(SnAs)_{0.4}(SiAs)_{0.6}$ alloy ended at point P_2 (Fig. 3), which corresponded to the four-phase peritectic transformation $L + SiAs_2 \leftrightarrow SnAs + SiAs$. Apparently, the duration of synthesis and annealing was insufficient for this transformation to be fully completed, and there was a certain amount of unreacted silicon diarsenide left. The lattice parameter of tin monoarsenide present in the alloys with the SnAs–SiAs cross section and calculated using XRD data was slightly different from the reference value; the parameters a and *b* of the SiAs monoclinic lattice were slightly increased, while the parameter *c* was slightly decreased (Table 2). It can be concluded that the solid-phase solubility along the SnAs–SiAs section was very low.

The Sn–SnAs–SiAs–Si trapezium could be divided into triangles that corresponded to the equilibrium of three solid phases using three methods (Fig. 1a, c, d). If option (c) is correct, the SiAs–Sn cross section separates silicon, and silicon should not be identified in alloys with the compositions in the concentration triangle (in the plane of the figure, to be precise) located above this cross section. If option (a) is correct, SnAs should not be identified in the alloys with the compositions in the concentration triangle located below the Sn_4As_3–SiAs cross section. The most informative solution to this problem was the study of the samples of the SnAs–Si cross section.

For example, we detected silicon in the $(SnAs)_{0.8}Si_{0.2}$ alloy by XRD, and its peaks were dominating (Fig. 2c), which makes the scheme presented in Fig. 1c incorrect. To choose between schemes (a) and (d), we must examine in more detail the paths of alloy crystallisation of the SnAs–Si polythermal section. Figure 3 shows two possible schemes of phase equilibria in a ternary system, corresponding to situations (a) and (d) in Fig. 1. The crystallisation processes proceeded similarly according to both schemes in the range of compositions rich in arsenic. The field of primary crystallisation of arsenic was limited by monovariant curves e_3P_1 and e_1P_1 along which the eutectic processes $L \rightarrow As + SnAs$ and

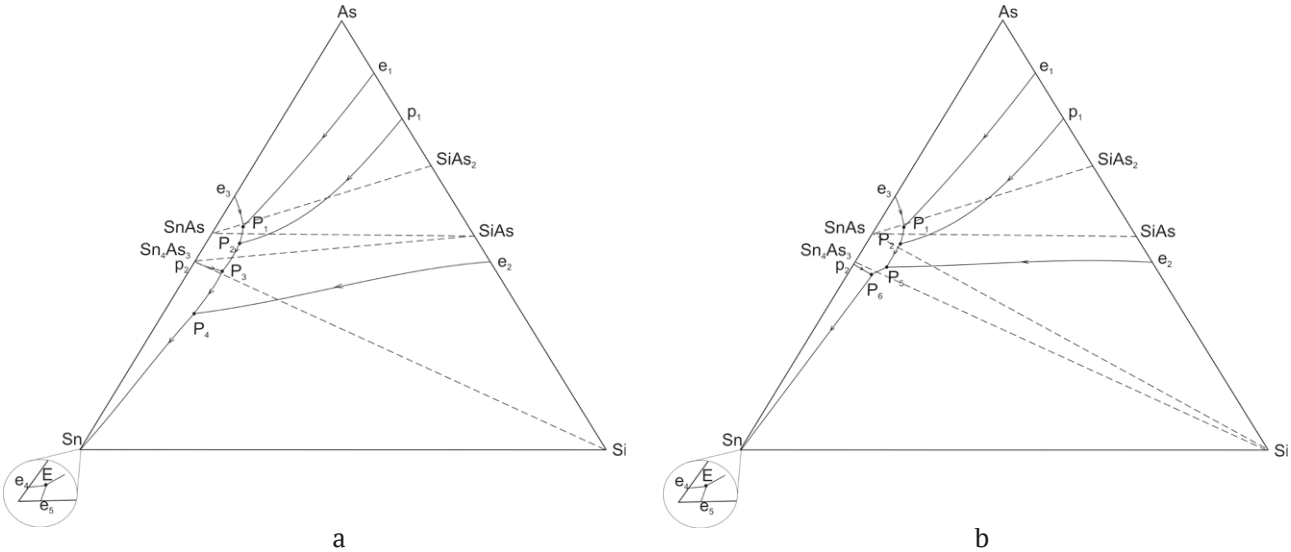

a b

Fig. 3. Schemes of phase equilibria in the Si–Sn–As ternary system

Table 2. Lattice parameters of silicon monoarsenide present in the alloys of the SnAs–SiAs section

PDF2 data		Composition of the alloys, mol f., SiAs				
SiAs		0.2	0.3	0.4	0.6	0.8
a, Å	15.97	15.979	15.980	15.976	15.977	15.979
b, Å	3.668	3.670	3.672	3.669	3.667	3.666
c, Å	9.529	9.520	9.526	9.527	9.526	9.526
β°	106.0	106.1	106.1	106.0	106.0	106.0

$L \rightarrow As+SiAs_2$ occurred, respectively. The four-phase peritectic equilibrium $L+As \leftrightarrow SnAs+SiAs_2$ corresponded to point P_1.

The peritectic process $L+SiAs \leftrightarrow SiAs_2$ occurred along the p_1P_2 curve, while the eutectic process $L \rightarrow SnAs + SiAs_2$ proceeded along the P_1P_2 curve. Curves e_1P_1, P_1P_2, and p_1P_2 limited the field of primary crystallisation of silicon diarsenide. The peritectic point P_2 corresponded to the invariant equilibrium $L + SiAs_2 \leftrightarrow SnAs + SiAs$.

Further processes were different for the two schemes. First, we will consider the option presented in Fig. 3a. Point P_3 corresponded to the four-phase equilibrium with the participation of the melt and solid phases $SnAs + SiAs + Sn_4As_3$, and it was also peritectic, as it was located outside the triangle connecting the compositions of solid phases coexisting in equilibrium. The $L \rightarrow SiAs + SnAs$ process proceeded along the P_2P_3 curve. The p_2P_3 curve separated the primary crystallisation fields of SnAs and Sn_4As_3.

The P_3P_4 curve separated the primary crystallisation fields of the Sn_4As_3 and SiAs phases. The eutectic process $L \rightarrow SiAs + Si$ proceeded along the e_2P_4 line and along the P_4E line: $L \rightarrow Sn_4As_3 + Si$. Point P_4 corresponds to the peritectic process $L + SiAs \rightarrow Sn_4As_3+Si$. Point E was located inside the triangle of solid phases and corresponded to the eutectic equilibrium $L \rightarrow Sn_4As_3 + Si + Sn$. It was degenerate, as the eutectics e_4 and e_5 in binary systems were degenerate.

In the second scheme (Fig. 3b), point P_5 corresponded to the non-variant peritectic process $L + SiAs \rightarrow SnAs+Si$, while point P_6 corresponded to the peritectic process $L + SnAs \rightarrow Sn_4As_3 + Si$. The processes similar to the first scheme occurred with a further decrease of temperature (Fig. 3a).

We will consider a possible sequence of crystallisation processes for the $(SnAs)_{0.8}Si_{0.2}$ alloy in accordance with the first scheme. The figurative point of the melt was located in the field of primary crystallisation of SiAs. Once silicon monoarsenide crystals were separated from the melt, secondary crystallisation occurred along the P_3P_4 curve, and the crystallisation process was completed at point P_4: $L + SiAs \rightarrow Sn_4As_3 + Si$. According to the second scheme (Fig. 3b), the $(SnAs)_{0.8}Si_{0.2}$ composition was in the field of primary silicon crystallisation, and once silicon was separated, the process occurred along the e_2P_5 line and completed with the peritectic process $L + SiAs \rightarrow SnAs + Si$.

Clear intense peaks of silicon and Sn_4As_3 were observed on the diffraction pattern of the $(SnAs)_{0.8}Si_{0.2}$, while peaks of tin monoarsenide were absent (Fig. 2c). Similar diffraction patterns were also obtained for samples of the SnAs–Si cross section that were richer in silicon, and only the intensity of the peaks changed. This allowed stating that the correct scheme is the one presented in Figs. 1a and 3a, according to which the subsolidus phase separation was performed by the $SnAs–SiAs_2$, SnAs–SiAs, Sn_4As_3–SiAs, and Sn_4As_3–Si. sections. The lattice parameter of silicon present in the alloys of the section varied within the range of experimental error and without any patterns. The calculated parameters of the rhombohedral lattice of Sn_4As_3 in a hexagonal device (Table 3) also did not allow

Table 3. Lattice parameters of the Sn_4As_3 phase present in the alloys of the SnAs–Si section

PDF2 data		Composition of the alloys, mol f., Si					
Sn_4As_3		0.1	0.2	0.3	0.4	0.6	0.8
a, Å	4.089(1)	4.088	4.086	4.086	4.090	4.078	4.088
c, Å	36.059(6)	36.081	36.0174	36.006	36.140	36.120	36.119

drawing a conclusion that a solid solution of any significant range was formed based on this compound.

We also studied several alloys of the SiAs–Sn polythermal section which did not participate in the subsolidus phase separation. This section crossed the Sn_4As_3–Si cross section, therefore the alloys with low and high tin content participated in different equilibria. X-ray phase analysis showed the presence of Sn_4As_3, Si, and SiAs phases in the $(SiAs)_{0.8}Sn_{0.2}$alloy (Fig. 4a), and Sn_4As_3, Si, and Sn phases in the $(SiAs)_{0.4}Sn_{0.6}$ alloy (Fig. 4b). This indicated that the process of crystallisation of the first alloy ended at point P_4, while the crystallisation of the second alloy ended at point E (Fig. 3a).

3.2. *Results of differential thermal analysis of alloys. Determining the temperatures of four-phase transformations*

In this work, differential thermal analysis was performed primarily to determine the temperature of four-phase equilibrium. It was impossible to plot T-x diagrams of polythermal cross sections and the projection of the liquidus surface of the ternary system using experimental data only, as the maximum heating temperature (1273 K) was limited both by the technical properties of the furnace and by the risk of depressurisation of Stepanov's quartz ampoules at high temperatures and arsenic vapour pressure. Therefore, liquidus was not achieved for all samples in the course of DTA.

Figure 5 shows thermograms of some alloys selected so that the temperature of the

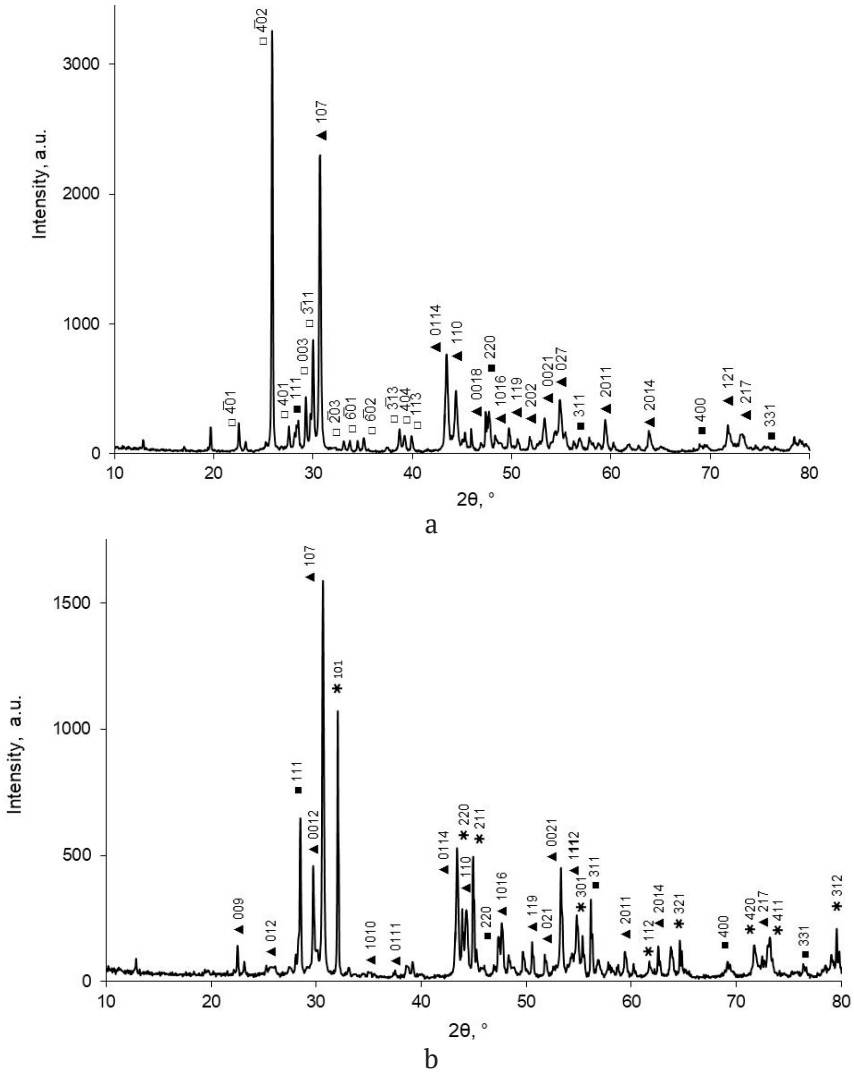

Fig. 4. X-ray powder diffraction patterns of the Si–Sn–As system: a – $(SiAs)_{0.8}Sn_{0.2}$; b – $(SiAs)_{0.4}Sn_{0.6}$. Phase symbols: ■ – Si, ⁎ – Sn, □ – SiAs, ▲ – Sn_4As_3

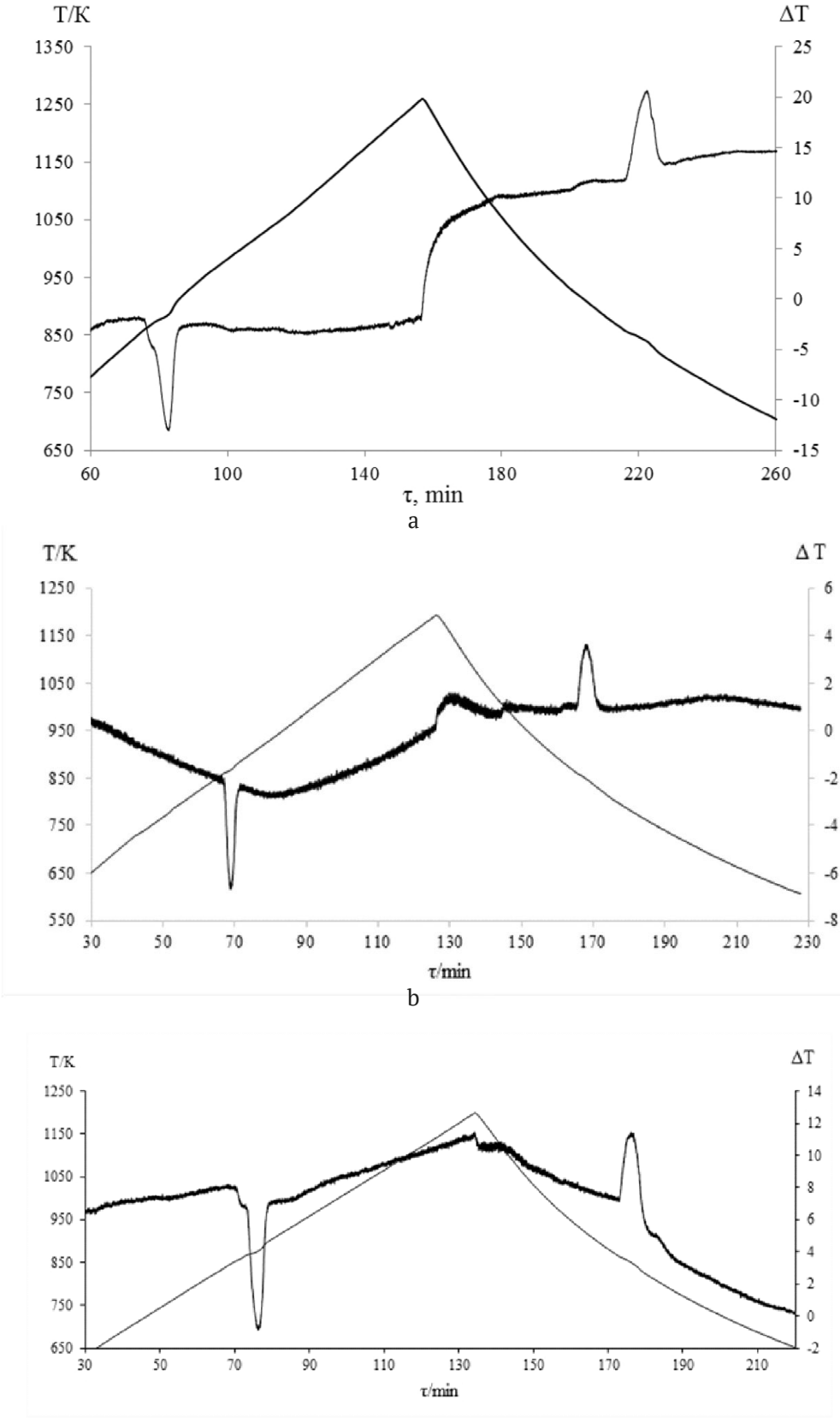

Fig. 5. Thermograms of alloys: a – $(SnAs)_{0.8}(SiAs_2)_{0.2}$; b - $(SnAs)_{0.4}(SiAs)_{0.6}$; c - $(SnAs)_{0.9}Si_{0.1}$; d - $(SiAs)_{0.9}Sn_{0.1}$; e - $(SiAs)_{0.4}Sn_{0.6}$

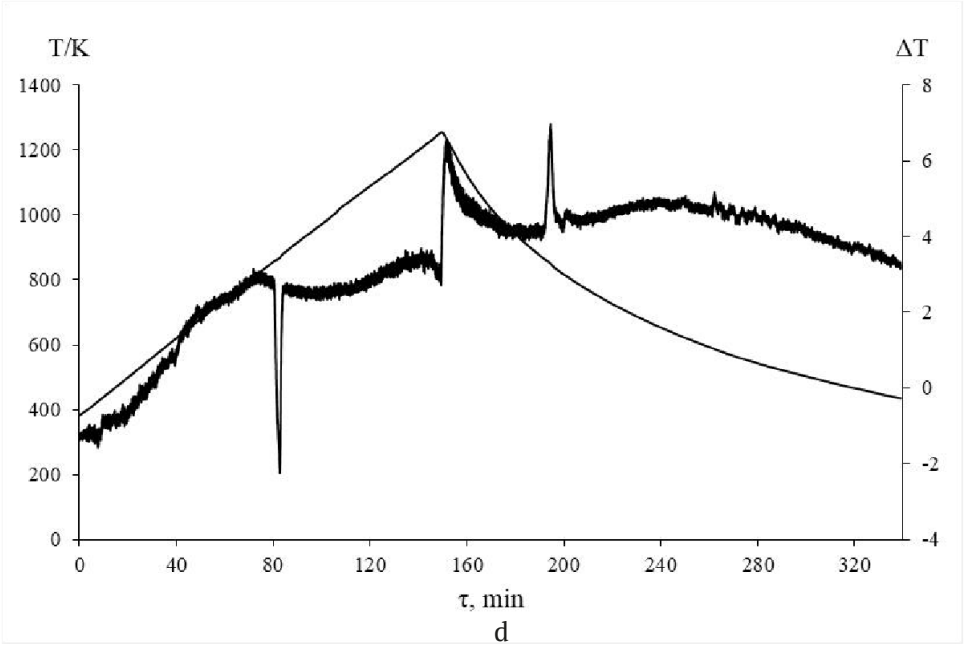

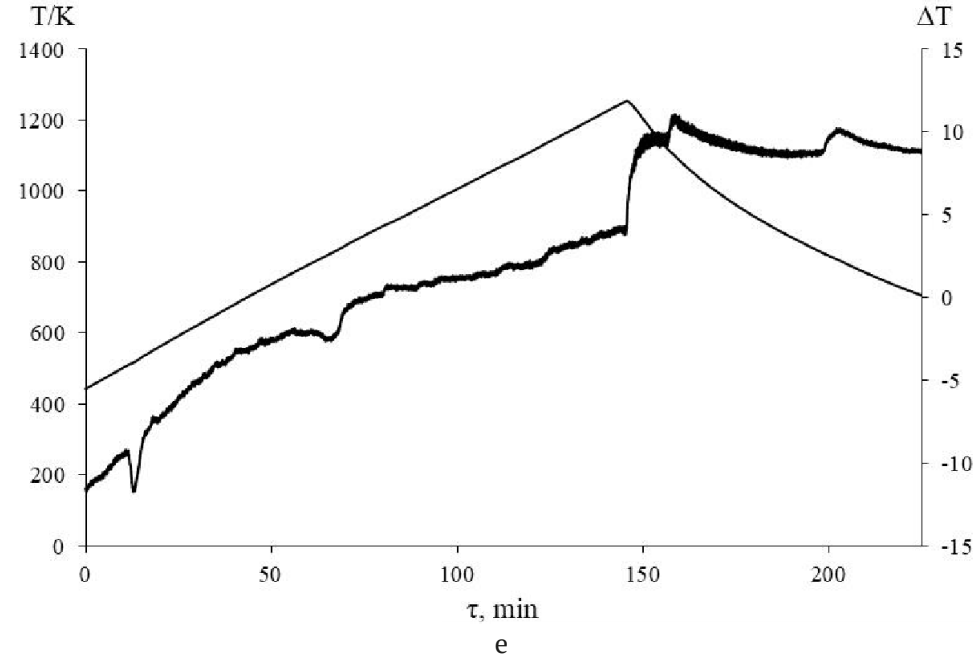

End of fig. 5

beginning of the first effect on the heating curve corresponded to the temperature of a certain four-phase invariant equilibrium. For instance, the crystallisation process ended at point P_1 for samples of the SnAs–$SiAs_2$ section, whose compositions were located to the left of the intersection point of this section with the p_1P_2 curve (Fig. 3a), On the thermogram of the alloy containing 20 mol. % silicon diarsenide, the temperature of the beginning of the first effect was 850±1 K (Fig. 5a), and this temperature corresponded to the four-phase process L + As ↔ SnAs+$SiAs_2$.

As for compositions located to the right of the intersection point of the SnAs–$SiAs_2$ section and the p_1P_2 curve, as well as for all alloys of the SnAs–SiAs section, crystallisation was completed at point P_2 with the process L + $SiAs_2$ ↔ SnAs + SiAs. For these alloys, we recorded the temperature of the beginning of the first endoeffect at 847±1 K (Fig. 5b shows the thermogram of the $(SnAs)_{0.4}(SiAs)_{0.6}$ sample).

We determined the temperature of the L + SnAs ↔ SiAs + Sn_4As_3 (p. P_3) peritectic process by thermography of $(SnAs)_{0.9}Si_{0.1}$ alloy. It was 845±1 K (Fig. 5c).

The temperature of peritectic transformation L + SiAs → Sn_4As_3 + Si (p. P_4) could be determined in the course of a thermographic study of the alloys that are rich in silicon of the SnAs–Si section, as well as of the alloys of the Sn–SiAs section with a high content of silicon monoarsenide. Fig. 5d presents a thermogram of the $(SiAs)_{0.9}Sn_{0.1}$ sample, and the determined temperature of the beginning of the first endoeffect was 840±1 K.

The crystallisation of the alloys of the Sn–SiAs section with a high content of tin ended at p. E (Fig. 3a) The temperature of the corresponding eutectic process L → Sn_4As_3 + Si + Sn was determined according to the DTA results of the $(SiAs)_{0.4}Sn_{0.6}$ alloy, and it amounted to 503±1 K (Fig. 5e), which is slightly lower than the temperature of tin melting.

4. Conclusions

We used X-ray diffraction analysis and differential thermal analysis to study the phase relations in the Si–Sn–As ternary system. It was established that the phase subsolidus demarcation was performed by the SnAs–$SiAs_2$, SnAs–SiAs, Sn_4As_3–SiAs, and Sn_4As_3–Si sections. Taking into account the theoretical analysis and XRD results, we suggested a scheme of phase equilibria in the system that presupposed the existence of one eutectic and four peritectic invariant equilibria with the participation of a melt and three solid phases. Differential thermal analysis allowed identifying the temperatures at which these four-phase equilibrium occurred: L + As ↔ SnAs + $SiAs_2$ (850±1 K); L + $SiAs_2$ ↔ SnAs + SiAs (847±1 K); L + SnAs ↔ SiAs + Sn_4As_3 (845±1 K); L + SiAs → Sn_4As_3 + Si (840±1 K); L → Sn_4As_3 + Si + Sn (503±1 K). According to the X-ray diffraction analysis, the solid phase solubility along the studied sections was very small, and a solid replacement solution with a range of at least 3 mol % was formed only based on tin monoarsenide along the SnAs–SiAs section. Further examination of the Si–Sn–As system presupposes a more detailed study of this issue as well as a construction of T-x diagrams of polythermal sections and projections of isotherms of the liquidus surface of the ternary system.

Contribution of the authors

The authors contributed equally to this article.

Conflict of interests

The authors declare that they have no known competing financial interests or personal relationships that could have influenced the work reported in this paper.

References

1. Ugai Ya. A., Miroshnichenko S. N., Goncharov E. G. Study of the *P-T-x* diagram of the Si-As system*. *Inorganic Materials*. 1974;10(10): 1774–1777. (In Russ.). Available at: https://www.elibrary.ru/item.asp?id=29085699

2. Ugai Ya. A., Popov A. E., Goncharov E. G., Lukin A. N., Samoilov A. M. Electrophysical properties and homogeneity region of germanium arsenide*. *Inorganic Materials*. 1983;19(2): 190–192. (In Russ.). Available at: https://www.elibrary.ru/item.asp?id=29095704

3. Goncharov E. G., Gladyshev N. F., Ugai Ya. A. Physicochemical nature of intermediate phases in the germanium – arsenic system*. *Russian Journal of Inorganic Chemistry*. 1977;22(7): 1951–1956. (In Russ.). Available at: https://www.eli-brary.ru/item.asp?id=29091830

4. Goncharov E. G., Popov A. E., Zavrazhnov A. Yu. Semiconducting phosphides and arsenides of silicon and germanium. *Inorganic Materials*. (In Russ.). 1995;31(5): 579–591. Available at: https://www.elibrary.ru/item.asp?id=29113633

5. Cheng A-Q., He Z., Zhao J., Zeng H., Chen R-Sh. Monolayered silicon and germanium monopnictide semiconductors: excellent stability, high absorbance, and strain engineering of electronic properties. *ACS Applied Materials & Interfaces*. 2018;10(6): 5133–5139. https://doi.org/10.1021/acsami.7b17560

6. Zhou L., Guo Y., Zhao J. GeAs and SiAs monolayers: Novel 2D semiconductors with suitable band structures. *Physica E: Low-dimensional Systems and Nanostructures*. 2018;95: 149–153. https://doi.org/10.1016/j.physe.2017.08.016

7. Ramzan M. S., Bacic V., Jing Y., Kuc A. Electronic properties of a new family of layered materials from groups 14 and 15: first-principles simulations. *The Journal of Physical Chemistry C*. 2019;123(41): 25470–25476. https://doi.org/10.1021/acs.jpcc.9b07068

8. Barreteau C., Michon B., Besnard C., Giannini E. High-pressure melt growth and transport properties of SiP, SiAs, GeP, and GeAs 2D layered semiconductors.

Journal of Crystal Growth. 2016;443(1): 75–80. https://doi.org/10.1016/j.jcrysgro.2016.03.019

9. Reddy P. V. S., Kanchana V., Millichamp T. E., Vaitheeswaran G., Dugdale S. B. Enhanced superconductivity in the high pressure phase of SnAs studied from first principles. *Physica B: Condensed Matter*. 2017;505: 33–40. https://doi.org/10.1016/j.physb.2016.10.026

10. Ma Z., Zhuang J., Zhang X., Zhou Zh. SiP monolayers: New 2D structures of group IV–V compounds for visible-light photohydrolytic catalysts. *Frontiers of Physics*. 2018;13(138104). https://doi.org/10.1007/s11467-018-0760-8

11. Shojaei F., Mortazavi B., Zhuang X., Azizi M. Silicon diphosphide (SiP_2) and silicon diarsenide ($SiAs_2$): Novel stable 2D semiconductors with high carrier mobilities, promising for water splitting photocatalysts. *Materials Today Energy*. 2020;16(100377). https://doi.org/10.1016/j.mtener.2019.100377

12. Kamali A. R., Fray D. J. Tin-based materials as advanced anode materials for lithium ion batteries: a review. *Reviews on Advanced Materials Science*. 2011;27: 14–24. Available at: https://www.elibrary.ru/item.asp?id=16869557

13. Kathleen L. *Synthesis and characterization of tetrel pnictides and compounds in the lithium-tetrel-arsenic system*. University of California. Davis ProQuest Dissertations Publishing: 2016. 136 p. Available at: https://www.proquest.com/openview/6c5577b9817fa2c2864fdeda33e2acfb/1?cbl=18750&diss=y&loginDisplay=true&pq-origsite=gscholar

14. Woo K. E., Dolyniuk J. A., Kovnir K. Superseding van der Waals with electrostatic interactions: Intercalation of Cs into the interlayer space of SiAs2. *Inorganic Chemistry*. 2019;*58*(8): 4997–5005. https://doi.org/10.1021/acs.inorgchem.9b00017

15. Semenova G. V., Goncharov E. G. *Solid solutions with the participation of elements of the fifth group**. Moscow: Izd. MFTI Publ.; 2000. 160 p. (In Russ.) Available at: https://www.elibrary.ru/item.asp?id=25882424

16. Kononova E. Y., Sinyova S. I., Semenova G. V., Sushkova T. P. Phase equilibria in the Sn–As–Ge and Sn–As–P systems. *Journal of Thermal Analysis and Calorimetry*. 2014;117(3): 1171–1177. https://doi.org/10.1007/s10973-014-3883-3

17. Olesinski R. W., Abbaschian G. J. The As–Si (arsenic-silicon) system. *Bulletin of Alloy Phase Diagrams*. 1985;6(3): 254–258. https://doi.org/10.1007/BF02880410

18. Gokcen N. A. The As-Sn (tin-arsenic) system. *Bulletin of Alloy Phase Diagrams*. 1990;11(3): 271–278. https://doi.org/10.1007/BF03029298

19. Kovnir K., Kolen'ko Y. V., … Shevelkov A. V. Sn_4As_3 revisited: Solvothermal synthesis and crystal and electronic structure. *Journal of Solid State Chemistry*. 2009;182(3): 630–639. https://doi.org/10.1016/j.jssc.2008.12.007

20. Olesinski R. W., Abbaschian G. J. The Si–Sn (silicon–tin) system. *Bulletin of Alloy Phase Diagrams;* 1984;5: 273–276. https://doi.org/10.1007/BF02868552

* *Translated by author of the article*

Information about the authors

Tatiana P. Sushkova, Cand. Sci. (Chem.), Associate Professor, Department of General and Inorganic Chemistry, Voronezh State University (Voronezh, Russian Federation).

https://orcid.org/0000-0003-1969-7082
sushtp@yandex.ru

Galina V. Semenova, Dr. Sc. (Chem.), Full Professor, Department of General and Inorganic Chemistry, Voronezh State University (Voronezh, Russian Federation).

https://orcid.org/0000-0003-3877-985X
semen157@chem.vsu.ru

Elena Yu. Proskurina, Cand. Sci. (Chem.), Assistant Lecturer, Department of General and Inorganic Chemistry, Voronezh State University (Voronezh, Russian Federation).

https://orcid.org/0000-0002-6149-1398
helko7@yandex.ru

Received 03.10.2022; approved after reviewing 01.11.2022; accepted for publication 15.11.2022; published online 25.06.2023.

Translated by Marina Strepetova
Edited and proofread by Simon Cox